

Pressure-Induced Switch of the Direction of the Unique Jahn–Teller Axis of the Chromium(II) Hexaqua Cation in the Deuterated Ammonium Chromium Tutton Salt

Christopher Dobe, Thierry Strässle, Fanni Juranyi, and Philip L. W. Tregenna-Piggott*

Laboratory for Neutron Scattering, ETH Zürich and Paul Scherrer Institute, CH-5232 Villigen PSI, Switzerland

Received February 2, 2006

Inelastic neutron scattering (INS) spectra are presented for chromium(II) Tutton salts, as a function of the temperature and pressure. Transitions are observed between the levels of the ${}^5A_g(C_i)$ ground term and the data modeled with a conventional $S = 2$ spin Hamiltonian. At 10 K and ambient pressure, the zero-field-splitting parameters of the ammonium salt, $(ND_4)_2Cr(D_2O)_6(SO_4)_2$, are determined as $D = -2.431(4) \text{ cm}^{-1}$ and $E = 0.091(4) \text{ cm}^{-1}$, evolving to $D = -2.517(4) \text{ cm}^{-1}$ and $E = 0.127(5) \text{ cm}^{-1}$ upon application of 7.5(1.0) kbar of quasi-hydrostatic pressure. By contrast, the change in the INS spectrum of the rubidium salt in this pressure range is comparatively minor. The results are interpreted using a 5E_g vibronic-coupling Hamiltonian, in which low-symmetry strain, perturbing the adiabatic potential-energy surface, is pressure-dependent. It is argued that, for the ammonium salt, the change with pressure of the anisotropic strain impinging upon the $[Cr(D_2O)_6]^{2+}$ cation is sufficient to cause a switch of the long and intermediate Cr–OD₂ bonds, with respect to the crystallographic axes.

1. Introduction

A major concern of chemistry and physics today is to conceive of devices based upon the manipulation of the physical properties of molecules, with spin-crossover complexes¹ and single-molecule magnets² being prominent among these. In principle, the deformation arising from the Jahn–Teller effect can also be utilized as a device for data storage on the molecular level. Theoretical work on copper(II)-doped magnesium oxide has suggested that the deformation of the copper hexaoxide moiety in this system could be controlled by the application of a magnetic field but only at very low temperatures in a near-perfect crystal.³ Pioneering work by Hitchman, Simmons, Augustyniak, Strauss, and others on the ammonium copper Tutton salt has demonstrated that the distortion direction of the $[Cu(D_2O)_6]^{2+}$ cation relative to the crystallographic axes can be manipulated by small changes in the temperature and pressure.^{4–8} The divalent cation lies on sites of C_i symmetry and interacts

with the ammonium and sulfate groups via a complex hydrogen-bonding network. The switching of the long axis of the Jahn–Teller distortion is concomitant with a rotation of the ammonium group,⁴ and irradiation in the region of the N–D stretching vibrations has also been demonstrated to induce the phase change.⁹ The fine balance between the two forms is evident from observations that the transition point can be tuned by the addition of impurities in the form of cations,^{10,11} anions,¹² and isotopic composition.¹³ One drawback of this system for practical applications is that molecular probes, such as EXAFS, are not sensitive to the distortion direction,¹⁴ and the change in the expectation

* To whom correspondence should be addressed. E-mail: philip.tregenna@psi.ch.

- (1) Hauser, A.; Amstutz, N.; Delahaye, S.; Sadki, A.; Schenker, S.; Sieber, R.; Zerara, M. *Struct. Bonding* **2004**, *106*, 81.
- (2) Gatteschi, D.; Sessoli, R. *Angew. Chem.* **2003**, *42*, 268.
- (3) Tregenna-Piggott, P. L. W. *Adv. Quantum Chem.* **2003**, *44*, 461.
- (4) Simmons, C. J.; Hitchman, M. A.; Stratemeier, H.; Schultz, A. J. *J. Am. Chem. Soc.* **1993**, *115*, 11304.

- (5) Hitchman, M. A.; Maaskant, W.; Plas, J. v. d.; Simmons, C. J.; Stratemeier, H. *J. Am. Chem. Soc.* **1999**, *121*, 1488.
- (6) Rauw, W.; Ahsbans, H.; Hitchman, M. A.; Lukin, S.; Reinen, D.; Schultz, A. J.; Simmons, C. J.; Stratemeier, H. *Inorg. Chem.* **1996**, *35*, 1902.
- (7) Augustyniak, M. A.; Krupski, M. *Chem. Phys. Lett.* **1999**, *311*, 126.
- (8) Dobe, C.; Carver, G.; Bürgi, H.-B.; Tregenna-Piggott, P. L. W.; McIntyre, G. J.; Augustyniak-Jablokow, M. A.; Riley, M. J. *Inorg. Chem.* **2003**, *42*, 8524.
- (9) Chen, Z.; Strauss, H. L. *J. Am. Chem. Soc.* **1998**, *120*, 8789.
- (10) Simmons, C. J.; Hitchman, M. A.; Stratemeier, H.; Astley, T. *Inorg. Chem.* **2000**, *39*, 4651.
- (11) Schultz, A. J.; Cowan, J. A.; Hitchman, M. A.; Stratemeier, H. *Acta Crystallogr. C.* **2005**, *61*, M234.
- (12) Simmons, C. J.; Stratemeier, H.; Hitchman, M. A.; Riley, M. J. *Inorg. Chem.* **2006**, in press.
- (13) Hathaway, B. J.; Hewat, A. W. *J. Solid State Chem.* **1984**, *51*, 364.

values of the electronic coordinates that accompany the Jahn–Teller switch is marginal. A more promising candidate for *JahnTelleronics* is the ammonium chromium(II) Tutton salt of formula $(\text{ND}_4)_2\text{Cr}(\text{D}_2\text{O})_6(\text{SO}_4)_2$. The $[\text{Cr}(\text{D}_2\text{O})_6]^{2+}$ cation has the $[\text{Ar}]3d^4$ electronic configuration, resulting in a ${}^5A_g(C_i)$ ground term that is split to second order by spin–orbit coupling. A Jahn–Teller switch, accompanied by a reorientation of the principal directions of the zero-field-splitting tensor, could be detected by the change in the magnetic moment at temperatures comparable to the zero-field splitting. Unlike the copper(II) analogue, a switch of the Jahn–Teller axes is not induced by isotopic substitution.¹⁵ However, a change in the Cr–OD₂ bond lengths as a function of zinc substitution has been reported,¹⁶ leading to the suggestion that the Jahn–Teller switch might be induced by the application of pressure.⁶ This hypothesis is confirmed by experimental measurements reported herein. Inelastic neutron scattering (INS) data are presented for the ammonium and rubidium Tutton salts as a function of the pressure and temperature. Changes in the zero-field-splitting parameters are related to the form of the Jahn–Teller potential-energy surface by way of ${}^5E\otimes e$ calculations, using parameters not dissimilar to those previously employed to model the switch of the Jahn–Teller axis in the copper(II) analogue.

2. Experimental Section

$(\text{ND}_4)_2\text{Cr}(\text{D}_2\text{O})_6(\text{SO}_4)_2$ and $\text{Rb}_2\text{Cr}(\text{D}_2\text{O})_6(\text{SO}_4)_2$ were prepared by methods previously described,¹⁷ and the purities of the salts checked by powder X-ray diffraction measurements. INS measurements were performed on the time-of-flight spectrometer FOCUS at Paul Scherrer Institute (PSI), Villigen, Switzerland.¹⁸ An incident wavelength of 5.32 Å was selected, yielding an energy-transfer window extending to $\sim 15\text{ cm}^{-1}$. The instrumental settings were configured for maximum resolution at the elastic peak. Measurements under quasi-hydrostatic pressure were conducted using a clamp cell described previously.¹⁹ The sample was finely ground and packed into the cell stepwise, alternating with the addition of several drops of Fluorinert FC-77 (Fluka) acting as the pressure-transmitting medium. Pressure was applied using a hydraulic ram. From previous measurements conducted on sodium chloride, the final pressure was estimated to be ~ 7.5 (1.0) kbar over the experimental temperature range. The cell was placed in a standard ILL orange cryostat, and data acquired between 10 and 200 K.

3. Results

In Figure 1 are shown INS spectra of $(\text{ND}_4)_2\text{Cr}(\text{D}_2\text{O})_6(\text{SO}_4)_2$ as a function of the temperature and pressure. In all

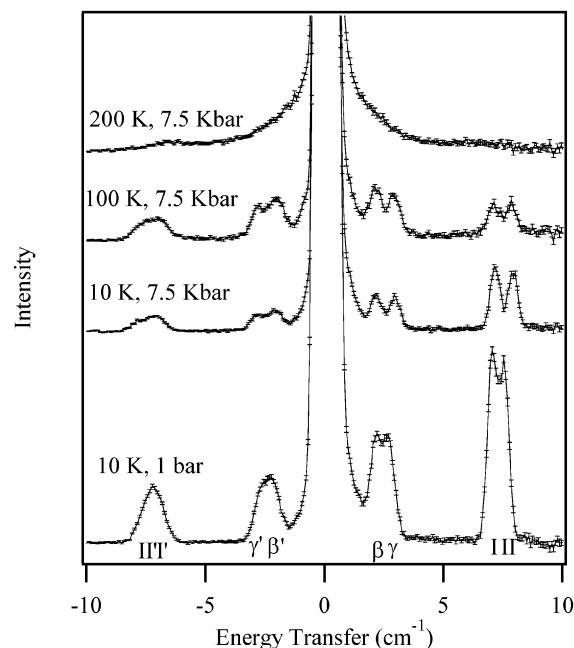


Figure 1. INS spectra of $(\text{ND}_4)_2\text{Cr}(\text{D}_2\text{O})_6(\text{SO}_4)_2$ as a function of the temperature and pressure, as indicated in the figure. The transitions are labeled according to the scheme in Figure 2.

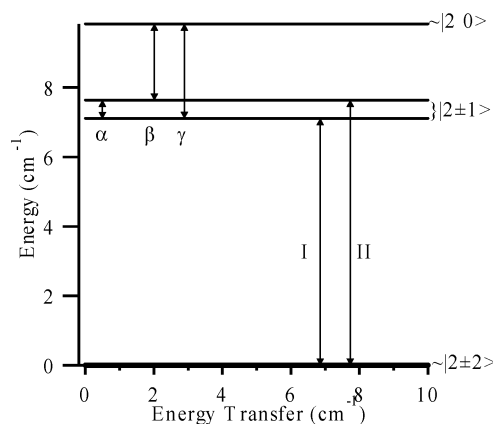


Figure 2. Energy-level diagram for an $S = 2$ system, corresponding to the observed transitions in $(\text{ND}_4)_2\text{Cr}(\text{D}_2\text{O})_6(\text{SO}_4)_2$. The INS transitions are indicated by arrows.

spectra, four INS transitions were observed, in a pattern of two doublets, commensurate with an energy-level diagram pertaining to an $S = 2$ spin system, shown in Figure 2. The transition α could not be resolved with the instrument settings used, being subsumed into the elastic band. The intensities were observed to decrease with increasing momentum transfer, Q , confirming the magnetic origin of the transitions.²⁰ As a result of the application of 7.5 kbar of quasi-hydrostatic pressure at 10 K, all transitions are shifted to higher energy, and the splitting of both doublets increases notably. Upon an increase in the temperature to 100 K while maintaining the sample under pressure, the bands broaden with little change in the peak positions. At 200 K, the broadening is excessive and the peak positions cannot be discerned. The dependence upon temperature of the INS spectrum of the pressure-induced form contrasts with that

(14) Masters, V. M.; Riley, M. J.; Hitchman, M. A. *Inorg. Chem.* **2001**, *40*, 843.

(15) Figgis, B. N.; Kucharski, E. S.; Reynolds, P. A. *Acta Crystallogr.* **1990**, *B46*, 577. Figgis, B. N.; Kucharski, E. S. *Acta Crystallogr.* **1991**, *C47*, 419.

(16) Araya, M. A.; Cotton, F. A.; Daniels, L. M.; Falvello, L. R.; Murillo, C. A. *Inorg. Chem.* **1993**, *32*, 4853.

(17) Dobe, C.; Noble, C.; Carver, G.; Tregenna-Piggott, P. L. W.; McIntyre, G. J.; Barra, A.-L.; Neels, A.; Janssen, S.; Juranyi, F. *J. Am. Chem. Soc.* **2004**, *126*, 16639.

(18) Mesot, J.; Janssen, S.; Holitzner, L.; Hempelmann, R. *J. Neutron Res.* **1996**, *3*, 293.

(19) Strässle, T.; Divis, M.; Ruzs, J.; Janssen, S.; Juranyi, F.; Sadykov, R.; Furrer, A. *J. Phys. Condens. Matter* **2003**, *15* (19), 3257.

(20) Carver, G.; Tregenna-Piggott, P. L. W.; Barra, A.-L.; Neels, A.; Stride, J. A. *Inorg. Chem.* **2003**, *42*, 5771.

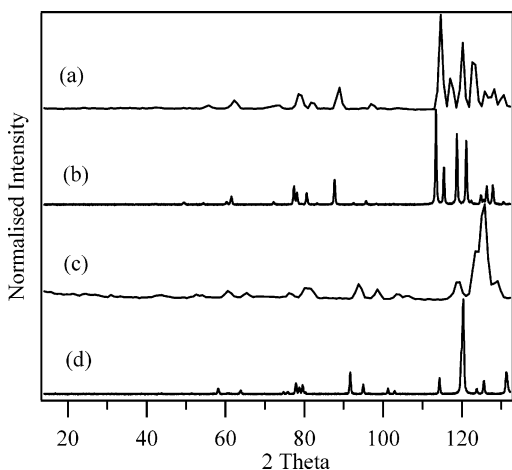


Figure 3. Experimental and theoretical diffraction patterns, measured and calculated with $\lambda = 5.32 \text{ \AA}$. Parts a and c display the diffraction patterns obtained for $(\text{ND}_4)_2\text{Cr}(\text{D}_2\text{O})_6(\text{SO}_4)_2$ on the FOCUS instrument, recorded at 10 K and ambient pressure and at 10 K and 7.5 kbar, respectively. Parts b and d display theoretical diffraction patterns calculated from crystallographic parameters determined for $(\text{ND}_4)_2\text{Cu}(\text{D}_2\text{O})_6(\text{SO}_4)_2$ at 15 K and ambient pressure and at 15 K and 1.5 kbar, respectively.⁴

recently reported at ambient pressure, where the spectrum can be observed at temperatures up to 297 K.¹⁷

The INS bands are assigned to transitions within the $^5\text{A}_g$ (C_2) ground term, split to second order by spin-orbit coupling. The zero-field splitting is conveniently described by the effective spin Hamiltonian, acting in a basis of the five $S = 2$ spin functions.

$$\hat{H}_s = D\left[\hat{S}_z^2 - \frac{1}{3}S(S+1)\right] + E[\hat{S}_x^2 - \hat{S}_y^2] \quad (1)$$

Least-squares fitting of the eigenvalues of eq 1, to the experimentally observed excitation energies at 10 K, yielded $D = -2.431(4) \text{ cm}^{-1}$ and $E = 0.091(4) \text{ cm}^{-1}$ for measurements at 1 bar, in close agreement with values previously reported,¹⁷ and $D = -2.517(4) \text{ cm}^{-1}$ and $E = 0.127(5) \text{ cm}^{-1}$ at 7.5 kbar. The degree of rhombicity, as measured by the ratio $|E/D|$, increases from 0.037(2) to 0.050(2) upon increasing pressure.

FOCUS is a versatile instrument from which a low-resolution diffraction pattern can also be recorded. The diffraction patterns obtained for $(\text{ND}_4)_2\text{Cr}(\text{D}_2\text{O})_6(\text{SO}_4)_2$ at 10 K and ambient pressure and at 10 and 7.5 kbar are shown in Figure 3. The data, though crude, clearly show that a phase transition has occurred, with the positions and relative intensities of the diffraction peaks changing markedly upon application of 7.5 kbar of pressure. Also shown are diffraction patterns calculated from crystallographic parameters previously derived for the copper analogue under similar experimental conditions.⁴ Save for a shift in the peak positions, the significance of which should not be overemphasized, the experimental diffraction patterns of the chromium salt mirror those calculated from the copper data, suggesting that the atomic positions are comparable. We may conclude, therefore, that the $(\text{ND}_4)_2\text{Cr}(\text{D}_2\text{O})_6(\text{SO}_4)_2$ salt also exhibits a switch of the long and intermediate Cr-OD₂ bond distances upon application of moderate pressure.

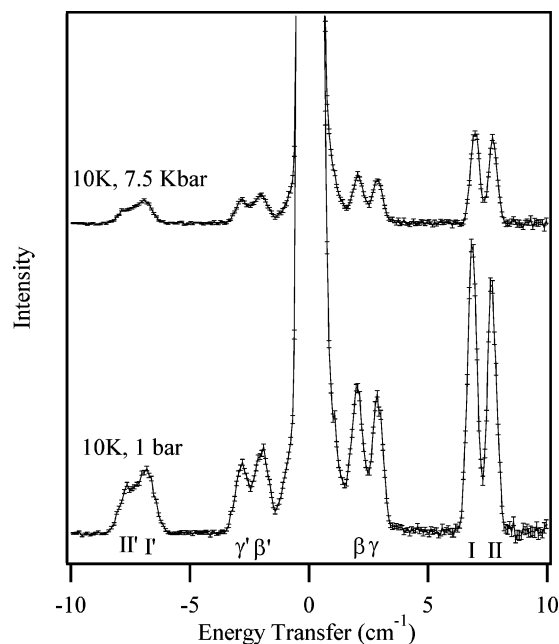


Figure 4. INS spectra for $\text{Rb}_2\text{Cr}(\text{D}_2\text{O})_6(\text{SO}_4)_2$ at 10 K at 1 bar and 7.5 kbar. The transitions are labeled following the scheme in Figure 2.

The analogous experiment was carried out on the rubidium salt, $\text{Rb}_2\text{Cr}(\text{D}_2\text{O})_6(\text{SO}_4)_2$, to ascertain the effect of pressure on the ground electronic structure of a system comparable to the ammonium salt but without the complication of a phase transition. Selected spectra are presented in Figure 4. At 1 bar, the splitting of the doublets is larger than that observed for the ammonium analogue, and this is reflected in the derived ground-state spin-Hamiltonian parameters of $D = -2.417(2) \text{ cm}^{-1}$ and $E = 0.140(4) \text{ cm}^{-1}$. Upon application of 7.5 kbar of pressure, the observed transitions shift to slightly higher energy, with a small reduction of the doublet splitting, resulting in minor changes to the ground-state spin-Hamiltonian parameters, documented along with the INS data in Table 1. A slight shift in the diffraction peak positions was observed upon application of pressure, consistent with a contraction of the unit cell.

Differential scanning calorimetry (DSC) measurements were performed on the ammonium chromium salt in an attempt to monitor the transformation back to the low-pressure phase, following a procedure identical with that carried out previously for the copper(II) analogue. The method consists of application of 450 bar of pressure at 298 K, cooling to 273 K, return of the sample environment to ambient pressure, and then monitoring the enthalpy change upon warming back to room temperature. However, the DSC measurements provided no intimation of a phase transition upon warming from 283 to 323 K. The failure to observe a back transformation in $(\text{ND}_4)_2\text{Cr}(\text{D}_2\text{O})_6(\text{SO}_4)_2$ under these conditions is not so surprising given the different structural chemistry of the two salts.^{4,15} It is likely that higher pressures are required, and the sample should be cooled to lower temperatures before releasing the pressure, necessitating the use of specialized DSC equipment not presently at our disposal.

Table 1. INS Transition Energies, Line Widths (Full Width at Half-Maximum), and the Derived Zero-Field-Splitting (ZFS) Parameters for (ND₄)₂Cr(D₂O)₆(SO₄)₂ and Rb₂Cr(D₂O)₆(SO₄)₂ at Various Temperatures and Pressures

| compound | pressure (bar) | temp (K) | transition energies (cm ⁻¹) | | | | fwhm I & II (cm ⁻¹) | ZFS parameters (cm ⁻¹) | |
|---|----------------|----------|---|----------|----------|----------|---------------------------------|------------------------------------|----------|
| | | | β | γ | I | II | | D | E |
| (ND ₄) ₂ Cr(D ₂ O) ₆ (SO ₄) ₂ | 1 | 10 | 2.14(2) | 2.71(2) | 7.041(8) | 7.565(8) | 0.48(1) | -2.431(4) | 0.091(4) |
| | 1 | 100 | 2.20(2) | 2.78(2) | 7.15(2) | 7.70(2) | 0.45(3) | -2.475(7) | 0.094(6) |
| | 7500 | 10 | 2.20(2) | 2.95(2) | 7.162(6) | 7.931(6) | 0.48(2) | -2.517(4) | 0.127(5) |
| | 7500 | 100 | 2.15(3) | 2.96(2) | 7.10(2) | 7.86(2) | 0.58(3) | -2.49(1) | 0.132(9) |
| Rb ₂ Cr(D ₂ O) ₆ (SO ₄) ₂ | 1 | 10 | 2.02(2) | 2.88(2) | 6.845(2) | 7.671(2) | 0.45(1) | -2.417(2) | 0.140(4) |
| | 7500 | 10 | 2.07(2) | 2.87(2) | 6.955(3) | 7.722(4) | 0.43(1) | -2.444(3) | 0.131(4) |

4. Theory

The INS data are interpreted with a ⁵E_g vibronic-coupling model as the interrelationship between the electronic and molecular structures of the [Cr(D₂O)₆]²⁺ cation evolves naturally from the eigenvalues and eigenvectors of the Hamiltonian.

The Hamiltonian for the problem is written as the sum

$$\hat{H} = \hat{H}_{\text{cub}} + \hat{H}_{\text{ph}} + \hat{H}_{\text{JT}} + \hat{H}_{\text{st}} \quad (2)$$

where H_{cub} and H_{st} designate the cubic and low-symmetry (strain) ligand-field contributions to the energy and H_{ph} and H_{JT} the phonon and Jahn–Teller coupling terms. The effective ⁵E_g (O_h) electronic Hamiltonian is written as

$$\hat{H}_{\text{cub}} = \frac{-b}{2}(\hat{U}_\theta \hat{S}_\theta + \hat{U}_\epsilon \hat{S}_\epsilon) \quad (3)$$

where

$$\hat{S}_\theta = \hat{S}_z^2 - \frac{1}{3}S(S+1); \quad S_\epsilon = \frac{1}{\sqrt{3}}(\hat{S}_x^2 - \hat{S}_y^2) \quad (4)$$

The parameter b has been derived previously, in the strong-field limit, and is a function of the Racah parameters B and C , the spin–orbit coupling parameter, ζ , and the octahedral splitting parameter, Δ_o .²¹ Formulating the ⁵E_g electronic Hamiltonian in the limit of a strong cubic field is a convenient but crude approximation that carries with it limitations on the significance of the parameters. In the following discussion, greater emphasis should be placed on the relative values of parameters employed to model different sets rather than the absolute values of the parameters themselves.

H_{ph} , the Hamiltonian for an e_g phonon mode before coupling, can be written as

$$\hat{H}_{\text{ph}} = [0.5\hbar\omega(\hat{P}_\theta^2 + \hat{P}_\epsilon^2 + \hat{Q}_\theta^2 + \hat{Q}_\epsilon^2)]\hat{U}_\tau \quad (5)$$

where $\hbar\omega$ is the phonon energy, \hat{Q}_i and \hat{P}_i are dimensionless operators, and anharmonic terms have been neglected. To second order, \hat{H}_{JT} has the form

$$\hat{H}_{\text{JT}} = A_1(\hat{Q}_\theta \hat{U}_\theta + \hat{Q}_\epsilon \hat{U}_\epsilon) + A_2[(\hat{Q}_\epsilon^2 - \hat{Q}_\theta^2)\hat{U}_\theta + 2\hat{Q}_\theta \hat{Q}_\epsilon \hat{U}_\epsilon] \quad (6)$$

where A_1 and A_2 are the first- and second-order Jahn–Teller coupling constants.

\hat{U}_θ , \hat{U}_ϵ , and \hat{U}_τ are electronic operators, active in the θ , ϵ orbital basis of the ⁵E_g ground term of the chromium(II) complex:

$$\hat{U}_\tau = \begin{pmatrix} 1 & 0 \\ 0 & 1 \end{pmatrix}, \quad \hat{U}_\theta = \begin{pmatrix} -1 & 0 \\ 0 & 1 \end{pmatrix}, \quad \hat{U}_\epsilon = \begin{pmatrix} 0 & 1 \\ 1 & 0 \end{pmatrix} \quad (7)$$

The term H_{st} models the low-symmetry ligand field imposed upon the [Cr(OH₂)₆]²⁺ cation, by the crystal forces, and has the explicit form

$$H_{\text{st}} = -e_\theta U_\theta + e_\epsilon U_\epsilon \quad (8)$$

Note that the phase of H_{st} is defined differently from that given previously.¹⁷ The following discussion is facilitated by redefining the anisotropic strain in polar coordinates, within the e_θ and e_ϵ coordinate frame:

$$\delta = (e_\theta^2 + e_\epsilon^2)^{1/2}$$

$$\varphi = \tan^{-1}(e_\epsilon/e_\theta) + \alpha; \quad \text{if } e_\theta > 0, \alpha = 0^\circ; \\ \text{if } e_\theta < 0, \alpha = 180^\circ$$

$$e_\theta = \delta \cos \varphi; \quad e_\epsilon = \delta \sin \varphi \quad (9)$$

The Hamiltonian was constructed as a matrix in the basis of the products of the 10 electronic states and the states of the { Q_θ , Q_ϵ } harmonic oscillator of dimension $N = 1/2(n_v + 1) - (n_v + 2)$, up to the level n_v . The matrix elements were evaluated, and the lowest-lying eigenvalues and corresponding eigenvectors found using a Lanczos diagonalization routine, as previously described.¹⁷ Theoretical zero-field-splitting parameters were calculated by fitting the eigenvalues of eq 1 to the five lowest-lying eigenvalues of eq 2. An analytical expression for the E_g Jahn–Teller potential surface is obtained by diagonalization of the 2×2 Hamiltonian matrices, omitting the terms in the kinetic energy and plotting the energy as a function of Q_θ and Q_ϵ . Contour plots were generated using Mathematica 5 and rendered with IGOR Pro 5.

When the term H_{st} is omitted from eq 2, the Hamiltonian possesses full cubic symmetry. The adiabatic potential-energy surface in the coordinate space of the two-dimensional vibration then has the familiar form of the warped “Mexican hat”, shown in Figure 5a, where we have employed vibronic-coupling parameters previously employed for the [Cr(OD₂)₆]²⁺ cation.¹⁷ The path of minimum energy along the angular coordinate, ϕ , shown as the top trace in Figure 6,

(21) Dobe, C.; Andres, H.-P.; Tregenna-Piggott, P. L. W.; Mossin, S.; Weihe, H.; Janssen, S. *Chem. Phys. Lett.* **2002**, *362*, 387.

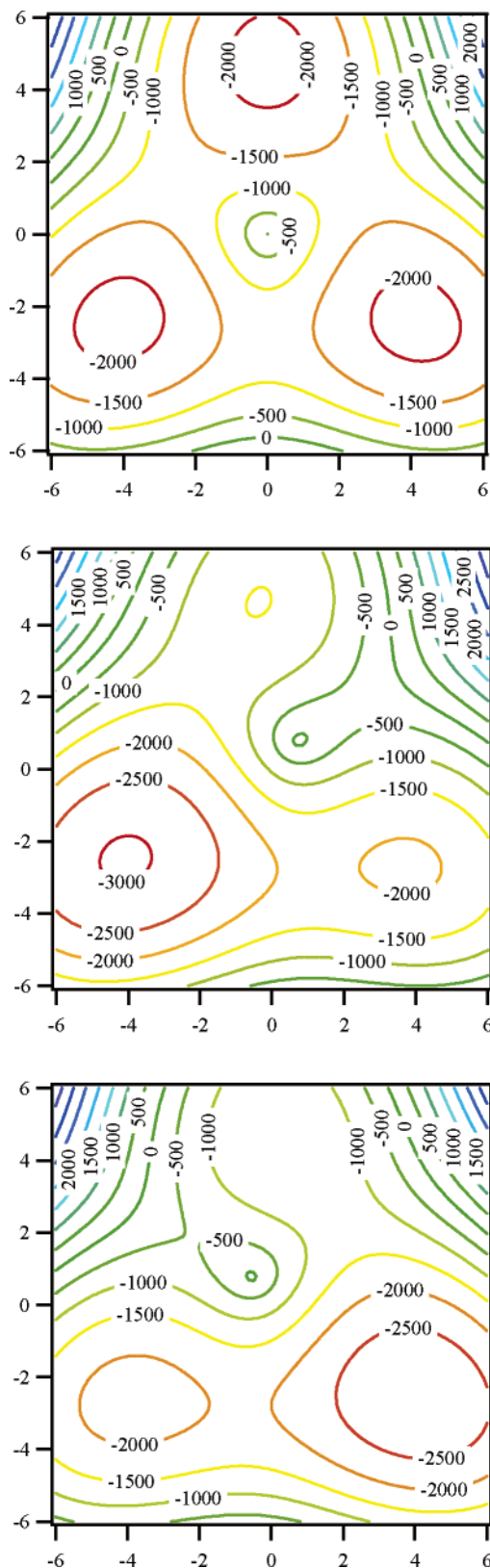


Figure 5. Contour plots of the ground-state Jahn–Teller potential-energy surface with Q_θ as the ordinate and Q_ϵ as the abscissa. All plots were calculated with $A_1 = -900 \text{ cm}^{-1}$, $A_2 = 33 \text{ cm}^{-1}$, and $\hbar\omega = 254 \text{ cm}^{-1}$. Top: $e_\theta = 0$ and $e_\epsilon = 0$ (cubic symmetry). Middle: $e_\theta = -700 \text{ cm}^{-1}$ and $e_\epsilon = 620 \text{ cm}^{-1}$ [(ND₄)₂Cr(D₂O)₆(SO₄)₂ at 1 bar]. Bottom: $e_\theta = -700 \text{ cm}^{-1}$ and $e_\epsilon = -450 \text{ cm}^{-1}$ [(ND₄)₂Cr(D₂O)₆(SO₄)₂ at 7.5 kbar].

exhibits three wells with minima at the cokernel points of D_{4h} symmetry located at $\phi = 0, 120,$ and 240° . The energy

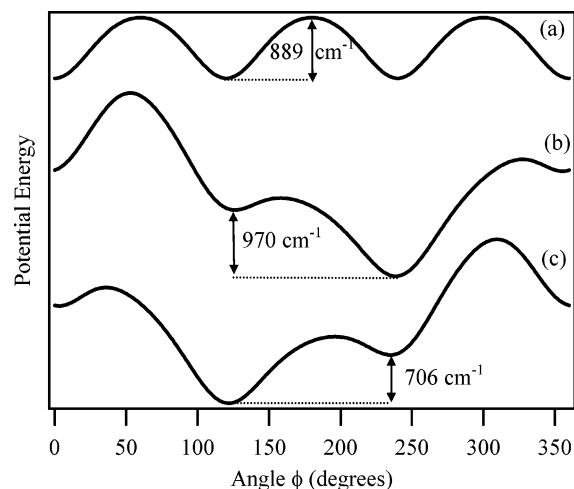


Figure 6. Plot of the potential-energy minimum around the warped “Mexican hat”, calculated with the parameters given in the caption of Figure 5: (a) cubic symmetry; (b) (ND₄)₂Cr(D₂O)₆(SO₄)₂, 1 bar; (c) (ND₄)₂Cr(D₂O)₆(SO₄)₂, 7.5 kbar.

difference between the minima and saddle points, 2β , is 889 cm^{-1} for this parameter set, being on the order of $2\beta \approx 2A_2(A_1/\hbar\omega)^2$.

The inclusion of anisotropic strain distorts the potential-energy surface, strongly influencing the bond lengths and spin-Hamiltonian parameters. The degree to which the strain induces a rhombic component to the electronic and molecular coordinates depends on the magnitude of δ relative to that of 2β and the directional nature of the strain, defined by the angular parameter φ . When $\delta \ll 2\beta$, the lowest minimum is localized at $\phi \approx 0^\circ$ for $-60^\circ < \varphi < 60^\circ$, $\phi \approx 120^\circ$ for $60^\circ < \varphi < 180^\circ$, and $\phi \approx 240^\circ$ for $180^\circ < \varphi < 300^\circ$. When $\delta \gg 2\beta$, the potential-energy minimum will be dictated by the strain, i.e., $\phi_{\min} \sim \varphi$. When $\delta \sim 2\beta$, the potential-energy surface is distorted but still retains the three potential wells. For a given strain, the minimum will be localized at a position close to $\phi = 0^\circ, 120^\circ,$ or 240° but will deviate toward the value φ . This situation pertains to the ammonium chromium Tutton salt. The INS spectrum is a sensitive measure of the value of ϕ_{\min} and is discussed together with this parameter in the following section. The spectrum is not sensitive to small changes in the magnitude of the Jahn–Teller distortion that might occur as a consequence of the phase transition. The Jahn–Teller radius is determined primarily by the linear Jahn–Teller coupling parameter, A_1 , which is kept at a fixed value for all calculations.

5. Discussion

The zero-field-splitting parameters derived for (ND₄)₂Cr(D₂O)₆(SO₄)₂ and Rb₂Cr(D₂O)₆(SO₄)₂ at 1 bar are in good agreement with those previously reported and, hence, can be modeled with vibronic-coupling parameters similar to those previously employed to model the electronic and molecular coordinates of these salts at ambient pressure.¹⁷ These parameters are presented in Table 2. The small change in the zero-field-splitting parameters of Rb₂Cr(D₂O)₆(SO₄)₂ observed when the pressure is increased to 7.5 kbar can, as expected, be modeled by a small increase in the isotropic

Table 2. Experimental and Theoretical Zero-Field-Splitting (ZFS) Parameters^a

| compound | pressure (bar) | temp (K) | experimental ZFS parameters (cm ⁻¹) | | theoretical ZFS and vibronic Hamiltonian parameters (cm ⁻¹) | | | | | | |
|---|----------------|----------|---|----------|---|----------|-----------------------|-----------------------|----------|----------------|----------------|
| | | | <i>D</i> | <i>E</i> | <i>D</i> | <i>E</i> | <i>e</i> _θ | <i>e</i> _ε | <i>d</i> | <i>φ</i> (deg) | Δ _O |
| Rb ₂ Cr(D ₂ O) ₆ (SO ₄) ₂ | 1 | 10 | -2.417(2) | 0.140(4) | -2.416 | 0.139 | -990 | 750 | 1242.0 | 217.1 | 11 910 |
| | 7500 | 10 | -2.444(3) | 0.131(4) | -2.443 | 0.132 | -950 | 800 | 1272.8 | 218.9 | 11 990 |
| (ND ₄) ₂ Cr(D ₂ O) ₆ (SO ₄) ₂ | 1 | 10 | -2.431(4) | 0.091(4) | -2.432 | 0.090 | -700 | 620 | 935.1 | 221.5 | 11 940 |
| | 7500 | 10 | -2.517(4) | 0.127(5) | -2.514 | 0.125 | -700 | -450 | 832.2 | 147.3 | 12 000 |

^a The theoretical values were calculated with $A_1 = -900$ cm⁻¹, $A_2 = 33$ cm⁻¹, $\hbar\omega = 254$ cm⁻¹, $B = 637$ cm⁻¹, $C = 2640$ cm⁻¹, $\zeta = 193.2$ cm⁻¹, and values for e_θ , e_ϵ , and Δ_O given in the table.

and anisotropic strains. The change in these parameters provides a guide as to what can be expected purely as a consequence of the pressure-induced lattice compression.

Calculations with strain parameters of $e_\theta = -700$ cm⁻¹ and $e_\epsilon = 620$ cm⁻¹ ($\delta = 935.1$ cm⁻¹ and $\varphi = 221.5^\circ$) provide a satisfactory account of the INS transition energies and Cr–OD₂ bond lengths determined from measurements on (ND₄)₂Cr(D₂O)₆(SO₄)₂ at 10 K and ambient pressure, with $|E/D| = 0.037$, $\phi_{\min} = 238.5^\circ$, and $\Delta_2 - \Delta_1 = 970$ cm⁻¹, the energy difference between the minima of the lowest-lying wells.

The ratio of $|E/D|$ in high-spin d⁴ complexes is determined primarily by two bonding considerations: (i) the π anisotropy and (ii) the rhombic distortion of the equatorial bond lengths. The π anisotropy is critical in determining the ground-state zero-field-splitting parameters of manganese(III) complexes but is less important for chromium(II) complexes, for reasons discussed earlier.²² Indeed, the ratio of $|E/D|$ for the [Cr(OH₂)₆]²⁺ cation in solution, measured by electron paramagnetic resonance (EPR), is negligibly small,²³ a result which we have corroborated by INS spectroscopy.²⁴ The increase in the ratio of $|E/D|$ in the high-pressure phase therefore implies that the ground state is localized at a position further away from points of cokernel D_{4h} symmetry on the Q_θ and Q_ϵ potential-energy surfaces.

Further information on the potential-energy surface is provided by the temperature dependence of the INS spectrum. In INS studies of high-spin chromium(II)^{17,21} and manganese(III)²⁵ compounds previously undertaken, the INS bands are noted to broaden as kT approaches Δ_2 , the energy of the next higher-lying potential-energy minimum, suggesting that relaxation processes such as phonon-assisted tunneling strongly influence the line widths. At ambient pressure, no broadening of the INS bands is noted in the 10–100 K temperature range, whereas at 7.5 kbar, the line widths of transitions I and II are 20% greater than their values at 10 K. The difference is even more striking at 200 K. The spectrum of (ND₄)₂Cr(D₂O)₆(SO₄)₂ at ambient pressure is well-resolved at this temperature,¹⁷ but at 7.5 kbar, the broadening is so excessive that the spectrum can no longer be discerned. This would suggest that, at 100 and 200 K,

the energy separation between the two lowest-lying wells is reduced in the high-pressure phase. We believe that this also holds true at 10 K, given the similarity of the INS transition energies in the 10 and 100 K spectra and their known sensitivity to the detailed form of the potential-energy surface.¹⁷

Reducing the value of e_ϵ to 450 cm⁻¹ while keeping e_θ constant at -700 cm⁻¹ equates to a reduction in the magnitude of the strain vector to $\delta = 832.2$ cm⁻¹ and a realignment of its angular direction to $\varphi = 212.7^\circ$. When these parameters are employed, the calculated value of $|E/D|$ increases to 0.05 while $\Delta_2 - \Delta_1$ is reduced to 706 cm⁻¹, in keeping with deductions based on the high-pressure INS data. A good agreement with the experimentally determined zero-field-splitting parameters can then be obtained by a small increase in Δ_O , comparable to that required to model the Rb₂Cr(D₂O)₆(SO₄)₂ data. The structural transition from the low- to high-pressure phase implies a permutation of the intermediate and long bond lengths due to a change in the lattice strain impinging upon the [Cr(OH₂)₆]²⁺ cation. Such a permutation requires a change in the sign of e_ϵ , such that $\varphi = 147.3^\circ$; the eigenvalues remain invariant. Experimental and calculated parameters are collected in Table 2.

Figure 5 displays potential-energy surfaces for (ND₄)₂Cr(D₂O)₆(SO₄)₂ in the low- and high-pressure phases, calculated with the parameters given in Table 2, with the paths of minimum energy along the angular coordinate, ϕ , shown as the middle and bottom traces in Figure 6. These plots summarize our conclusions concerning the transformation that takes place at 10 K upon application of pressure. The switch of the order of the two lowest-lying minima implies a switch of the long and intermediate Cr–OD₂ bond lengths with respect to the crystallographic axes. The calculated value of $\phi_{\min} = 122.0^\circ$ for the high-pressure phase deviates more from the point of cokernel symmetry compared to the value proffered for the low-pressure phase counterpart. A consequence of this is a tiny increase in the calculated difference between the intermediate and short Cr–OD₂ bond lengths (~ 0.003 Å) but a notable increase in the ratio $|E/D|$. We have deliberately chosen parameters that lead to a reduction in $\Delta_2 - \Delta_1$ for the high-pressure phase. This deduction is tentative, being based solely on a comparison of the variation of the INS line widths with temperature. If the energy gap $\Delta_2 - \Delta_1$ is indeed reduced upon application of pressure, then the derived Cr–OD₂ bond lengths, obtained from a diffraction experiment, should begin to converge at lower temperature.⁵

(22) Tregenna-Piggott, P. L. W.; Weihe, H.; Barra, A.-L. *Inorg. Chem.* **2003**, *42*, 8504.

(23) Telsler, J.; Pardi, L. A.; Krzystek, J.; Brunel, L.-C. *Inorg. Chem.* **1998**, *37*, 5769. Telsler, J.; Pardi, L. A.; Krzystek, J.; Brunel, L.-C. *Inorg. Chem.* **2000**, *39*, 1834.

(24) Dobe, C.; Tregenna-Piggott, P. L. W., unpublished results.

(25) Basler, R.; Tregenna-Piggott, P. L. W.; Andres, H.; Dobe, C.; Gudel, H.; Janssen, S.; McIntyre, G. J. *J. Am. Chem. Soc.* **2001**, *123*, 3377. Thut, M.; Carver, G.; Tregenna-Piggott, P. L. W., manuscript in preparation.

5. Summary and Outlook

This work has demonstrated that the ammonium chromium Tutton salt undergoes a pressure-induced phase transition, a manifestation of which is a switch of the intermediate and long Jahn–Teller axes of the $[\text{Cr}(\text{OD}_2)_6]^{2+}$ cation with respect to the crystallographic axes. The INS data suggest a greater degree of rhombicity in the high-pressure phase and a reduction in the energy gap between the two lowest-lying potential-energy wells. At temperatures comparable to the zero-field splitting, a pronounced difference in the magnetic anisotropy of the two phases should occur, on account of the anticipated reorientation of the principal directions of the zero-field-splitting tensor and the different cooperative arrangements of the two crystallographically distinct hexaqua cations within the unit cell.⁵ This should now be confirmed

by single-crystal magnetochemical measurements. Experiments are currently in progress on $(\text{ND}_4)_2\text{Cr}(\text{D}_2\text{O})_6(\text{SO}_4)_2$ doped with zinc(II) to investigate the effect of chemically induced internal pressure on the detailed electronic structure, with preliminary data suggesting that the degree of rhombicity may itself be tuned by adjusting the zinc concentration.

Acknowledgment. We are very grateful to Denis Sheptyakov for his assistance in analyzing the crystallographic data and to Graham Carver for the programs used to calculate the potential-energy surfaces. We also thank Dr. Stan Hoffman for pointing out the importance of phonon-assisted tunneling in dictating EPR and INS line widths. This work was funded by the Swiss National Science Foundation.

IC060187G